www.sciencedirect.com www.em-consulte.com

IRBM

ELSEVIER MASSON

IRBM 33 (2012) 223–226

Original article

# MedataWeb: A shared platform for multimodality medical images and Atlases

## *MeDataWeb : une plateforme partagée pour l'imagerie médicale multimodalité et les atlas*

N. Betrouni *, N. Makni , A.-S. Dewalle-Vignion , M. Vermandel

*Inserm, U703 THIAIS, université Nord de France, CHRU de Lille, 152, rue du Docteur-Yersin, 59120 Lille, France*

Received 29 March 2012; received in revised form 6 April 2012; accepted 6 April 2012
Available online 22 May 2012

**Abstract**

Computer-assisted medical interventions and treatment planning have known an increasing interest and research activity in different fields and applications. However, before the routine deployment of these procedures becomes a reality, in vivo and in silico validations must be undertaken. This paper describes a platform containing multimodality medical images and atlases useful for algorithms evaluation, comparison and validation. The platform contains des-identified data (images, contours and atlases) from the ProstateAtlas and ProstateWeb project: the first morphological and zonal atlas of the prostate, and from clinical data of lymphoma PET (PETWeb). Data are available at the URL: http://www.medataweb.U703.net.


**Résumé**

Les gestes médicaux-chirurgicaux assistés par l'imagerie, la simulation et la robotique ont connu un intérêt et un développement grandissants ces dernières années. Cependant, avant que l'utilisation de ces techniques en routine clinique devienne une réalité, elles doivent être validées (in silico, ex vivo, in vivo…). Cet article décrit une plateforme contenant des images médicales multimodalité et des atlas utiles pour l'évaluation d'algorithmes, la comparaison et la validation de méthodes. La plateforme contient des données anonymisées (images, les contours et atlas) du projet ProstateAtlas et ProstateWeb : le premier atlas morphologique et zonale de la prostate. Il contient également des images de TEP de lymphome et les structures délimitées associées (PETWeb). Les données sont disponibles à l'adresse URL : http://www.medataweb.U703.net.


## 1. Introduction

In many clinical procedures, imaging takes an increasingly growing position and image analysis has become crucial. Starting from this observation and from the ubiquitous need for 3D data set with well-known ground truth to validate image processing tools/algorithms/methods, our motivation was to build an open and shared base containing images: clinical or/and simulated for different organs and modalities that could be used for this purpose. Such solution has been already proposed for brain [1]. The brain phantom combines a model and MR imaging simulator and is publicly available (www.bic.mni.mcgill.ca/brainweb). Based on the same concept, a full segmentation validation engine from the Laboratory Of Neuro Imaging (LONI – University of California, Los Angeles) has been recently described [2]. This solution offers a complete online solution for brain segmentation validation for dedicated application in Neurology (http://sve.loni.ucla.edu/).

Such databases remain rare for other anatomical localizations or applications. Only a statistical atlas of prostate cancer distribution was recently proposed by Shen et al. [3] for optimizing biopsies. This database is also free and can be retrieved from the authors' website (www.rad.upenn.edu/sbia/projects/prostate.html).

In the next sections, we describe two datasets corresponding to clinical applications where imaging plays an important role. The first is dedicated to prostate cancer imaging. The second contains non-Hodgkin's lymphoma PET imaging including multi-expert manual delineations and automatic segmentation approaches.

* Corresponding author.
*E-mail address:* n-betrouni@chru-lille.fr (N. Betrouni).

1959-0318 
http://dx.doi.org/10.1016/j.irbm.2012.04.003

## 2. ProstateAtlas and ProstateWeb

From a morphologic point of view, the prostate is an exocrine gland, shaped like a pyramid with an upward base. The zonal anatomy of the prostate has been described for the first time in the 1960s, but the use of terms in anatomical practice was introduced in the 1980s [4]. It is composed of four zones: peripheral zone (PZ), central zone, transition zone (TZ) and fibromuscular structure (Fig. 1). PZ and TZ are key structures, as 70% of prostate tumours are located within PZ. Inversely, benign hypertrophy (BPH) most often occurs in the TZ, which becomes larger with age.

From a radiologic point of view, for men aged over 50 years, only two areas of the prostate are considered: the central gland (hypertrophied TZ and peri-urethral glands) and PZ. In this study, we assume that TZ refers to the central zone. As shown by Fig. 1, TZ is surrounded by the PZ, whose thickness and size depend on patient's age and prostate pathological symptoms, like BPH. The PZ is surrounded by vessels and is very likely to host irregular tissues like tumours.

Here we report the data and the models used to create the numerical phantom of the gland, the PZ and the TZ. These materials and methods were published in Betrouni et al. [5].

Briefly, we propose clinical magnetic resonance (MR) images of 30 selected patients. Images consist of axial T1-weighted sequence (65 to 85 images, voxel size $0.48 \times 0.48 \times 1.3\,\text{mm}^3$). An expert radiologist manually segmented the images to delineate the prostate gland, the PZ, the TZ, urethra, cysts and tumours (Fig. 1). Images are provided in DICOM format and contours are provided in DICOM RTSS format.

This data was used in [5] to create atlases for the prostate, the peripheral and TZs.

Creation of the models and atlases was done is following way:

- structures delineation by an expert;
- creation of mesh files for each structure;
- creation of binary files from the meshes;
- statistical description of shapes;
- probabilistic description of the two zones. This description allows to take into account the inter-patients variability and could be incorporated as an *a priori* knowledge in an automatic segmentation process.

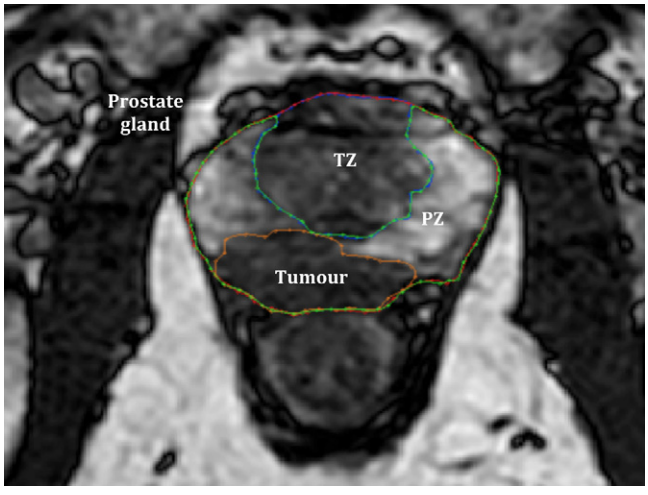


Fig. 1. T1W axial MR image of prostate with delineation of prostate gland, peripheral zone (PZ), transition zone (TZ) and tumour in the peripheral zone.

We also provide for each patient mesh and binary files for each structure (gland, PZ and TZ). Binary data are provided in two formats: as DICOM files and as Raw files. Mesh files described as Level sets, are in the object file format (OFF) (Fig. 2).

The last part of this data concerns the atlases. The first atlases are morphological atlases of the prostate, the PZ and the TZ. They were created using principal components analysis (PCA). The second class of atlases are probabilistic atlases describing zonal distribution of two zones: PZ and TZ inside the prostate gland (Fig. 3).

Files are provided in the Analyze (.hdr, .img) file format.

## 3. PETWeb

[18F]-Fluorodeoxyglucose PET ([18F]-FDG PET) has become an essential technique in oncology for initial staging, treatment planning and assessment of therapeutic response. The most challenging and crucial step is to correctly determine the metabolic tumor volume in order to provide more accurate target volume definition in radiotherapy treatment planning. Accurate and reproducible manual delineation is difficult on PET images due to the poor spatial resolution of the PET imaging which results in a gradual transition between healthy tissue and tumor. Numerous (semi) automatic methods have been proposed and evaluated. The evaluations are usually performed on phantom, on simulated data or/and on anatomopathological data with the corresponding ground truths being well established. For clinical data without available ground truth, the evaluation is made through comparisons with the volume segmented on morphological images or with expert(s) manual delineation(s). Comparisons of the performance of some methods sometimes complete evaluations.

In Dewalle et al. [6], we proposed an assessment framework based on comparisons with manual delineations performed by experts. Applied on clinical data with non-Hodgkin's lymphoma, this framework allows to determine, among the five considered methods, the one that provides results closest to the manual delineations set, performed by five experts [6]. In this purpose, data had to be collected.

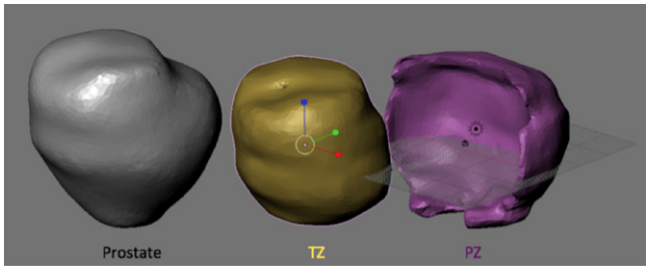


Fig. 2. An example of mesh files for the three structures: prostate, peripheral zone (PZ) and the transition zone (TZ) described as level sets and provided in the Object File Format.

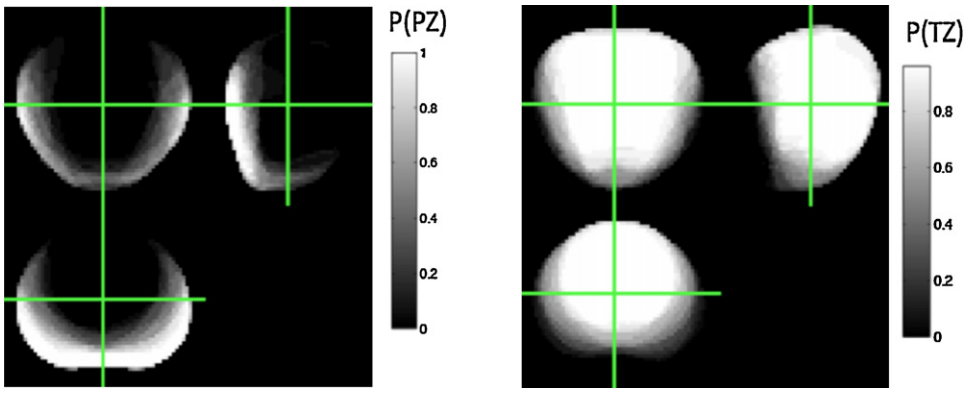


Fig. 3. Probabilistic distribution of the peripheral zone (left) and the transition zone (right).

Given the time required to perform the manual delineations and to make the methods work (implantation, calibration. . .), the online distribution of these data appears to be of great interest for community. In fact it makes it possible to easily and without loss of time for data collection evaluate any new method of segmentation by comparison with a set of manual delineations and by comparison with the five considered methods.

After a brief description of data collection in Section 3.1, the modalities of this distribution are described in Section 3.2.

### 3.1. Data collection

#### 3.1.1. Clinical data

The PET images were acquired on a GE Advance PET tomograph (General Electric Medical Systems, Milwaukee, Wisconsin, USA) from 20 patients with non-Hodgkin's lymphoma. The therapeutic response of these patients treated by radio-immunotherapy was assessed through [18F]-FDG-PET at 6 weeks, 12 weeks, and 6 months compared with the baseline scans. The transaxial resolution in the 2D mode, measured according to the National Electrical Manufacturers Association protocol using the standard acquisition parameters, was 4.2 mm (5.5 and 7.4 mm, respectively) at the center of the field of view (at 10 and 20 cm, respectively). A whole-body image scan was started 1 h after the injection of a 370 MBq activity of [18F]-FDG. For each bed position, a 5-min emission scan and a 2-min transmission scan (external source of germanium) were performed. For each acquisition, data were reconstructed in transverse slices (202 slices; slice thickness, 4.3 mm; matrix, $128 \times 128$; pixel size, $4.3 \times 4.3\,mm^2$). Reconstruction parameters were 2 iterations/28 subsets (iterative reconstruction algorithm: OSEM) with a scatter correction (convolution subtraction) and a decay correction.

#### 3.1.2. Tumor selection

For each of the 20 patients, one tumor was selected from the PET images. This selection was made to ensure easy lesion identification and to exhibit variability in size, shape, and intensity.

#### 3.1.3. Manual delineations

The 20 selected lesions were manually delineated three times by five qualified nuclear medicine physicians with no prior segmentation training. Manual delineations were performed, slice-by-slice, on reconstructed coronal PET images. Assessment of consistency in contouring was visually performed. Each expert delineated all the 20 lesions one after another first before performing the second and then the third delineation. Fifteen manual delineations were thus performed for each of the 20 lesions.

#### 3.1.4. Automatic segmentations

Five segmentations methods, we used in previous studies [7,8], were considered:

- the commonly used in daily practice application of a threshold of 42% of the maximum SUV (the so-called 42% threshold-based approach);
- the contrast-oriented method proposed by Nestle et al. [9]. This thresholding method, increasingly mentioned in studies, uses a threshold depending linearly on a measure of the activity of the lesion and on a measure of the background activity;
- the method proposed by Daisne et al. [10]. Validated with surgical specimens, this method is based on a relationship between source to background ratio and the threshold be used;
- the widely used application of the fuzzy C-means algorithm directly to the PET images;
- the maximum of intensity projections (MIP)-based method proposed by Dewalle-Vignion et al. [7,8]. This method uses (1) the MIP algorithm to overcome the usually poor PET image contrast and (2) a possibility theory-based algorithm to take account for uncertainty related to the gradual transition between healthy tissues and lesions, partially due to the poor spatial resolution of the images.

The calibration steps required by the Nestle and the Daisne methods were performed using an in-house phantom.

Application of these five methods to the manually defined volumes encompassing the lesions enables five automatic segmentations to be associated with each of the 20 lesions.

### 3.2. Data distribution

In summary, the generated data set included for each lesion:

- the 15 manual delineations (five senior nuclear physicians × 3 times) (Fig. 4);
- the automatic segmentation obtained by the 42% threshold-based approach;
- the automatic segmentation obtained by the contrast-oriented method of Nestle et al. [9];
- the automatic segmentation obtained by the Daisne et al. method [10];
- the automatic segmentation obtained by the MIP-based method [6,7];
- the automatic segmentation obtained by the application of the fuzzy C-means algorithm directly to the PET images.

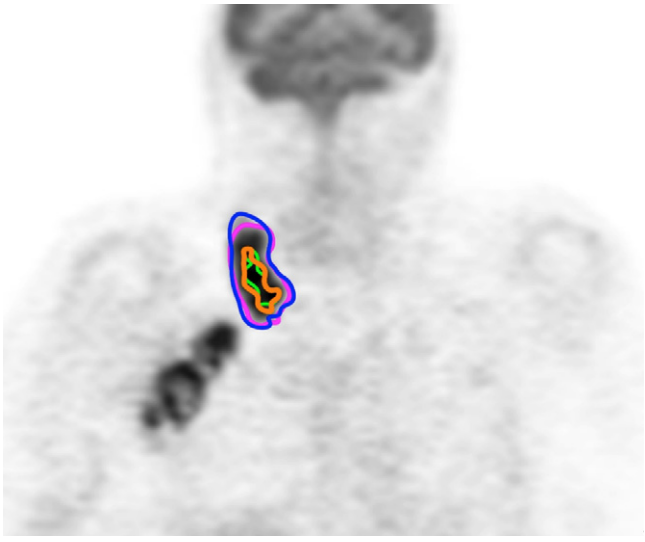

Fig. 4. Overview of manual delineations available for PET images (four delineations from four different experts).


Fig. 5. Snapshot of the homepage of the web server.

Associated with the PET DICOM images, these 20 delineations per lesion are provided in two formats: DICOM RT-STRUCT files and Raw files.

The result of any new method of segmentation applied to the PET DICOM images can then be compared with the corresponding DICOM RT-STRUCT files or Raw files.

## 4. Conclusion

Constructing and using digital phantoms present the benefit to provide ground truth to optimize, control or validate different image based procedures. This paper presents a shared database containing clinical and simulated images from different modalities and for different localizations.

These datasets are publicly available through a web server (Fig. 5) (http://www.medataweb.U703.net) and constitute a global framework for validation and comparison of these procedures. This platform remains open to others anatomical localizations and should be updated soon by simulated Magnetic Resonance Angiography of the cerebral vascular tree.

## References

[1] Collins DL, Zijdenbos AP, Kollokian V, Sled JG, Kabani NJ, Holmes CJ, et al. Design and construction of a realistic digital brain phantom. IEEE Trans Med Imaging 1998;17(3):463–8.
[2] Shattuck DW, Prasad G, Mirza M, Narr KL, Toga AW. Online resource for validation of brain segmentation algorithms. Neuroimage 2009;45(2):431–9.
[3] Shen D, Lao Z, Zeng J, Zhang W, Sesterhenn IA, Sun L, et al. Optimized prostate biopsy via statistical atlas of cancer spatial distribution. Med Image Anal 2004;8:139–50.
[4] McNeal JE. The zonal anatomy of the prostate. Prostate 1981;2:35–49.
[5] Betrouni N, Iancu A, Puech P, Mordon S, Makni N. ProstAtlas: a digital morphologic atlas of the prostate. Eur J Radiol 2012 [under press], http://dx.doi.org/10.1016/j.ejrad.2011.05.001.
[6] Dewalle-Vignion AS, Yeni N, Petyt G, Verscheure L, Huglo D, Béron A, et al. Evaluation of PET volume segmentation methods: comparisons with expert manual delineations. Nucl Med Commun 2012;33(1):34–42.
[7] Dewalle-Vignion AS, Betrouni N, Lopes R, Huglo D, Stute S, Vermandel M. A new method for volume segmentation of PET images, based on possibility theory. IEEE Trans Med Imaging 2011;30:409–23.
[8] Dewalle-Vignion AS, Makni N, Betrouni N, Huglo D, Stute S, Buvat I, et al. Nouvelle méthode de segmentation des volumes d'intérêt en TEP : utilisation de la théorie des possibilités. IRBM 2011;32(6): 351–62.
[9] Schaefer A, Kremp S, Hellwig D, Rube C, Kirsch CM, Nestle U. A contrast-oriented algorithm for FDG-PET-based delineation of tumour volumes for the radiotherapy of lung cancer: derivation from phantom measurements and validation in patient data. Eur J Nucl Med Mol Imaging 2008;35(11):1989–99.
[10] Daisne JF, Sibomana M, Bol A, Doumont T, Lonneux M, Grégoire V. Tridimensional automatic segmentation of PET volumes based on measured source-to-background ratios: influence of the reconstruction algorithms. Radiother Oncol 2003;69(1):247–50.